Structural Correlations in Porous Silica: Molecular Dynamics Simulation on a Parallel Computer

Aiichiro Nakano, Lingsong Bi, Rajiv K. Kalia, and Priya Vashishta

Concurrent Computing Laboratory for Materials Simulations, Department of Physics and Astronomy, Department of Computer Science, Louisiana State University, Baton Route, Louisiana 70803-4001

(Received 9 November 1992; revised manuscript received 2 April 1993)

Molecular dynamics simulations of porous silica in the density range 2.2–0.1 g/cm^3 are carried out on a 41 472 particle system using a multiple instruction multiple data computer. The internal surface area, pore surface-to-volume ratio, pore size distribution fractal dimension, correlation length, and mean particle size are determined as a function of the density. Structural transition between a condensed amorphous phase and a low-density porous phase is characterized by these quantities. Various dissimilar porous structures with different fractal dimensions are obtained by controlling the preparation schedule and temperature.

PACS numbers: 61.43.Bn, 61.20.Ja

In recent years there has been a growing interest in porous materials because of their many technologically important applications. Much of the recent work has focused on aerogel silica, a form of porous SiO_2 which is prepared by hypercritical drying of an alcoholic silica gel [1]. It is an environmentally safe material with a large thermal resistance which makes it a suitable alternative to chlorofluorocarbon foamed plastic in thermal insulation of commercial and household refrigerators [1]. Aerogel silica is also a highly desirable material for passive solar energy collection devices because of its high optical transmission and large thermal resistance [1]. Other applications of porous glasses include catalysis and chemical separation [2]: Solid catalysts such as porous glasses are environmentally safer than other catalysts because they hold their acidity internally. A novel application of porous glasses is in the arena of optical switching, where porous materials are used as embedding frameworks for quantum-confined semiconducting microclusters [3]. These applications of porous glasses result from their unique selective separation capabilities, molecular transport, thermal resistance, and mechanical properties. All of these characteristics depend crucially on structural correlations such as the pore size, internal surface area, surface-to-volume ratio, and interface texture.

Structural correlations in porous silica span many hierarchical regimes. The short-range (<4 Å) correlations are known to arise from the structure of the SiO_4 tetrahedral unit [4]. The intermediate-range (4–8 Å) correlations, manifested as the first sharp diffraction peak (FSDP) in neutron- and x-ray diffraction experiments, arise from the connectivity of the tetrahedral units [5–7]. Both these correlations exist at normal density as well as in low-density amorphous silica. Beyond the intermediate range, small-angle neutron scattering (SANS) [8,9] and small-angle x-ray scattering [10,11] experiments on porous silica reveal a fractal structure.

In diffraction data, however, scatterings from different hierarchical regimes are mixed, and the interpretation of the data is sometimes difficult. On the other hand, molecular dynamics (MD) simulations enable the direct investigation of structural correlations by providing all the atomic coordinates. Microscopic modeling of structural correlations in porous silica requires large system sizes because the hierarchical regimes cover several decades of length scale. With the recent emergence of high-performance parallel computer architectures, it is now feasible to carry out large-scale atomistic simulations spanning the necessary length scales.

In this paper, we present the results of MD simulations for porous SiO_2 at densities in the range 2.2–0.2 g/cm^3. These simulations have been performed on an in-house distributed-memory multiple instruction multiple data computer [12]—an eight-node Intel iPSC/860. The systems we have simulated consist of 41 472 Si and O atoms. Even at the lowest density, 0.1 g/cm^3, the length of the MD box (240 Å) covers all the hierarchical correlation regimes mentioned above. Simulations reported here took 1200 hours on the iPSC/860 system.

The simulations are based on an effective interatomic potential which combines two-body and three-body interactions [4,13]. The two-body potential includes steric effects, the Coulomb interaction due to charge transfer, and charge-dipole interaction caused by electronic polarizabilities of atoms. The three-body potential takes into account the effect of covalency. Using these interatomic potentials, MD simulations have recently been performed for molten, crystalline, and amorphous states of normal SiO_2 and also permanently densified amorphous SiO_2. The simulation results for pair distribution functions, static structure factors, vibrational densities of states, and bond-angle distributions are in good agreement with neutron diffraction and nuclear magnetic resonance measurements [4,14].

On the iPSC/860, a highly efficient implementation of MD simulations has been achieved through a domain-decomposition scheme [15]. Interparticle interactions [16] have been calculated with a multiple-time-step approach which is implemented with the aid of a linked-list scheme. For a 41 472-particle system, this MD implementation yields 3070 time steps per hour on the eight-node iPSC/860. The parallel efficiency of this algo-

0031-9007/93/71(1)/85(4)$06.00

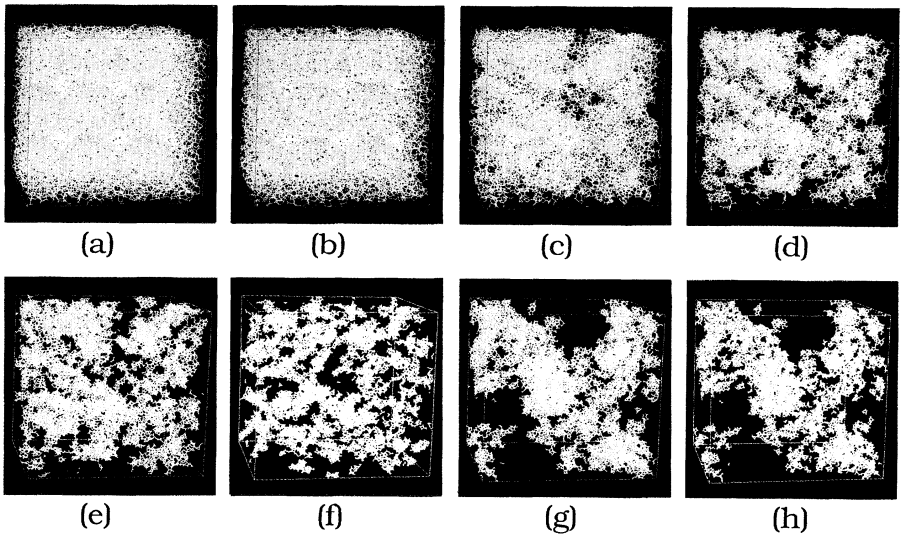

FIG. 1. Snapshots of MD porous SiO_2 glasses at densities (a) 2.2, (b) 1.6, (c) 0.8, (d) 0.4, (e) 0.2, and (f) 0.1 g/cm^3 prepared at 300 K, and (g) 0.2 and (h) 0.1 g/cm^3 prepared at 1000 K. Yellow lines represent Si-O bonds.

rithm is 0.97.

The porous SiO_2 systems are prepared as follows [17]. Starting with a well thermalized glass at the normal glass density 2.2 g/cm^3 and room temperature, porous glasses are obtained by successive expansions. At each expansion step, the coordinates of all the particles in the system are uniformly enlarged by a factor of 1.02–1.26 and subsequently the system is thermalized for 30000 time steps. During the thermalization, temperature is kept at 300 K by removing heat from the system. Next, with a conjugate gradient (CG) scheme, the system is brought into a local minimum-energy configuration [18]. In the relaxed configuration, particles are assigned random velocities according to the Maxwell distribution centered around 200 K. The equipartition of the energy is rapidly achieved (within 1000 time steps) and the temperature drops to 100 K. At each density, statistical averages are calculated over 9000 time steps.

Figure 1 displays snapshots of atomic positions of porous silica. At the condensed amorphous phase above 1.6 g/cm^3, the amorphous system possesses only short- and intermediate-range correlations; see Figs. 1(a) and 1(b). However, as the density is lowered below 1.6 g/cm^3, density fluctuations that give rise to pores of various sizes set in. A close examination of these snapshots [Figs. 1(c)–1(f)] reveals self-similarity at length scales in the range 5–25 Å.

In Fig. 2, we show a log-log plot of the pair distribution function $g(r)$ at various densities. Short-range correlations manifest themselves as peaks at distances less than 5 Å. Some of the peaks split at lower densities, but the peak positions change very little over the entire range of density. At the normal density, the first peak is located at 1.62 Å. However, at lower densities, there is an additional peak at 1.58 Å due to the Si-O bond inside a triangle unit. The number of these triangular units grows as the density is lowered. In the range 5–25 Å, a power-law decay is superimposed on the peak structures. From the power law, the fractal dimension d_f is calculated as $d_f = 3 + d\log[g(r)]/d\log(r)$ [17]. The power-law decay extends up to the correlation length, $r = \xi$, and at a larger length scale the material is homogeneous so that $g(r) = 1$ [8–11].

Figure 3(a) shows the neutral structure factor [4] $S_N(q)$ calculated from the MD configurations. The fractality is exhibited as a power-law behavior, $S_N(q) \propto q^{-d_f}$, in the range $\xi^{-1} < q < a^{-1}$ [19], where a is interpreted as the mean diameter of the structural units of the fractal network [8,11].

In Fig. 3(b) we compare the neutron structure factors of amorphous SiO_2 at normal density and porous glass at 0.1 g/cm^3. At 0.1 g/cm^3, the FSDP, a manifestation of

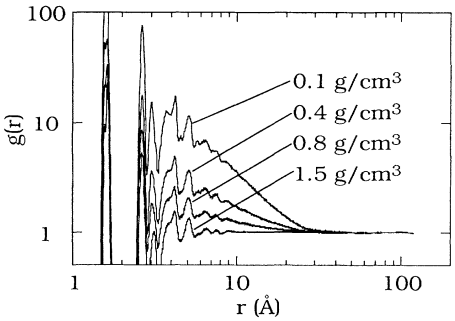

FIG. 2. Log-log plot of pair distribution functions $g(r)$ of silica glasses at densities at 0.1, 0.4, 0.8, and 1.5 g/cm^3 at 300 K.

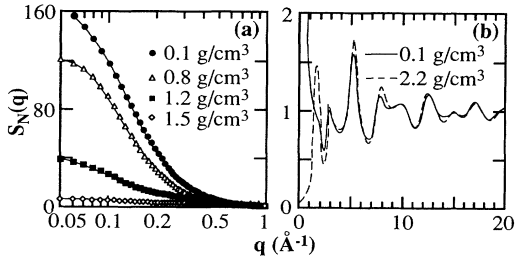

FIG. 3. (a) Semilog plot of neutron structure factors $S_N(q)$ at densities 0.1, 0.8, 1.2, and 1.5 g/cm^3. (b) $S_N(q)$ at densities 0.1 and 2.2 g/cm^3. The porous glasses are prepared at 300 K.

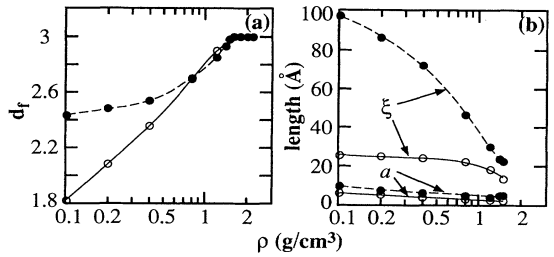

FIG. 4. (a) MD results on fractal dimension as a function of density. Open circles are for MD configurations prepared at room temperature 300 K, while solid circles are for 1000 K. (b) MD results on correlation length ξ and mean-particle size a as a function of density. Open and solid symbols have the same meaning as in (a).

intermediate-range order, is replaced by a shoulder with a superimposed power-law decay. This is consistent with the behavior of the pair distribution function where a power-law decay is superimposed on the peaks in the range 4–8 Å. Unlike the normal density glass, where the connectivity of tetrahedral units over distances ≤ 8 Å gives rise to the intermediate-range correlations, in porous glasses there is more free volume into which the network of tetrahedral and triangular units can grow. Therefore, the correlations continue to grow until there is no more free volume available at a length scale ~ 25 Å.

In Fig. 4(a), the solid curve shows the MD results on the density dependence of the fractal dimension d_f [20]. At 1.6 g/cm^3, d_f suddenly begins to deviate from 3. This density corresponds to the tensile limit of SiO_2 glass [17]. In Fig. 4(b), solid curves show the MD results on the density dependence of the correlation length ξ and the mean-particle size a. ξ increases slightly with decreasing density, while a changes little.

In real materials, d_f, ξ, and a depend on the aggregation process and sample preparation conditions such as pH value [8–11]. To investigate the effect of kinetic processes, we performed another set of MD simulations where temperature was kept at 1000 K instead of 300 K during the expansion process. Figures 1(g) and 1(h) show the snapshots of the resulting glasses at densities 0.2 and 0.1 g/cm^3, respectively. Larger d_f and more extended range of fractality (i.e., larger ξ/a) are observed; see dashed curves in Fig. 4. Kinetic processes during the expansion determine the structure of the resulting glass. After an expansion, each particle or cluster of particles searches for an energy minimum through its diffusive motion subject to the local interparticle correlation. Here, the balance between diffusion and local correlation is the most crucial factor to determine the structure. For higher temperatures, larger diffusion overcomes the correlation in immediate neighbors and more global configuration space is sought. As a result, energetically favored packed networks with larger d_f are formed. By controlling the balance between diffusion and correlation via temperature and expansion schedule, various dissimilar porous glasses with different d_f can be produced in MD simulations. This is contrary to kinetic modelings of aggregation processes [21] where only a few values of the fractal dimension are obtained depending on the rules used in the models.

Internal surface area S and pore surface-to-volume ratio S/V are the most important parameters characterizing the geometric features of a porous glass [2]. These parameters are calculated as follows: First we divide the MD box into cubes of the same size (length of the edge $l=4$ Å). We then determine for each cell whether it is occupied by particles or not. Pore volume is calculated as the number of unoccupied cells times l^3. On the other hand, internal surface area is calculated by summing up the area of interfaces between an occupied and an unoccupied cube. In Fig. 5, open circles represent the internal surface area as a function of density. Below the tensile limit, the internal surface increases rapidly as the density is lowered. At the same time, as shown by solid circles, the surface-to-volume ratio, which roughly estimates the inverse of the average pore size, decreases rapidly. The

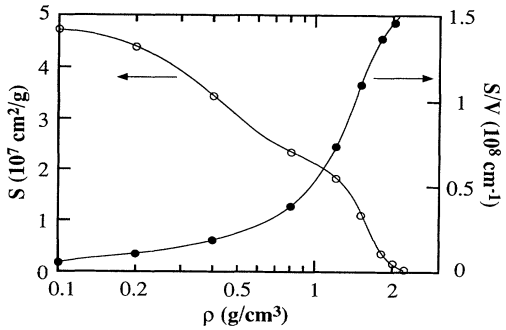

FIG. 5. Internal surface area S versus density calculated from the MD configurations (open circles). Pore surface-to-volume ratio S/V versus density calculated from the MD configurations (solid circles). The porous glasses are prepared at 300 K.

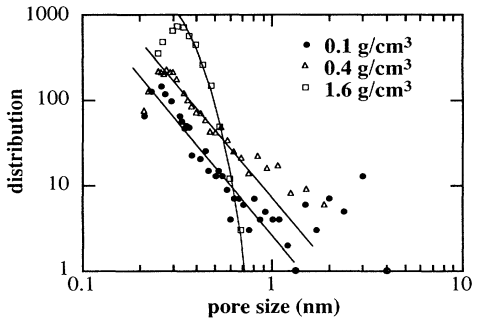

FIG. 6. Pore size distributions at densities 0.1, 0.4, and 1.6 g/cm^3. The porous glasses are prepared at 300 K. For 1.6 g/cm^3, the Gaussian fitting is shown by a solid line. For 0.1 and 0.4 g/cm^3, power-law fittings are shown by solid lines.

calculated density dependence of S is in good agreement with experiments [1].

Figure 6 shows the pore size distributions calculated from MD configurations. The MD box is again divided into cubes of size l, and their occupations are determined. The number of pores of size l is calculated as the number of unoccupied boxes which are isolated and do not share any face with other unoccupied boxes. In a condensed phase at 1.6 g/cm^3, the distribution is fitted as Gaussian, as shown in Fig. 6. Below the tensile limit, there are pores of all sizes, and the pore-size distribution exhibits a power-law decay. Fitting the distribution to l^{-b}, we get $b=2.7$ for densities 0.4 and 0.1 g/cm^3. The large fluctuation of the data beyond 1 nm is a finite-size effect.

In conclusion, using high-performance parallel architecture we have carried out large-scale MD simulations of porous silica to provide insight into the microscopics of the SANS data. Structural transition between a condensed amorphous phase and a low-density porous phase is characterized. In MD simulations, various dissimilar porous structures can be prepared by controlling the expansion schedule and temperature.

This work was supported by the U.S. Department of Energy, Office of Energy Research, Basic Energy Science, Materials Science Division, Grant No. DE-FG05-92ER45477. The computations were performed using the eight-node iPSC/860 in the Concurrent Computing Laboratory for Materials Simulations (CCLMS) at Louisiana State University. The facilities in the CCLMS were acquired with the Equipment Enhancement Grants awarded by the Louisiana Board of Regents through Louisiana Education Quality Support Fund (LEQSF).

[1] J. Fricke, J. Non-Cryst. Solids **121**, 188 (1990); **147 & 148**, 356 (1992).
[2] J. M. Drake and J. Klafter, Phys. Today, **43**, No. 5, 46 (1990).
[3] G. D. Stucky and J. E. MacDougall, Science **247**, 669 (1990).
[4] P. Vashishta *et al.*, Phys. Rev. B **41**, 12197 (1990).
[5] S. C. Moss and D. Price, in *Physics of Disordered Materials,* edited by D. Adler, H. Fritzsche, and S. R. Ovshinsky (Plenum, New York, 1985), p. 77.
[6] L. E. Busse and S. R. Nagel, Phys. Rev. Lett. **47**, 1848 (1981).
[7] S. Susman *et al.*, Phys. Rev. B **43**, 11076 (1991).
[8] T. Freltoft *et al.*, Phys. Rev. B **33**, 269 (1986).
[9] R. Vacher *et al.*, Phys. Rev. B **37**, 6500 (1988); J. Non-Cryst. Solids **106**, 161 (1988); J. Pelous *et al.*, *ibid.* **145**, 63 (1992).
[10] D. W. Schaefer and K. D. Keefer, Phys. Rev. Lett. **56**, 2199 (1986).
[11] T. Lours *et al.*, J. Non-Cryst. Solids **121**, 216 (1990).
[12] P. J. Denning and W. F. Tichy, Science **250**, 1217 (1990).
[13] We are also testing an interatomic potential which is adjusted to local environment, following A. Alavi *et al.*, Philos. Mag. B **65**, 489 (1992).
[14] S. Susman *et al.*, Phys. Rev. B. **43**, 1194 (1991).
[15] R. K. Kalia *et al.* (to be published); A. Nakano *et al.* (to be published).
[16] In the simulations reported here, a slightly modified interatomic potential has been used, which gives the same structural and dynamical properties as described in Refs. [4] and [14]. This was done to achieve higher speed up in large systems.
[17] J. Kieffer and C. A. Angell, J. Non-Cryst. Solids **106**, 336 (1988).
[18] We developed a CG algorithm which uses the second derivative of the potential energy and achieved a speed up of factor 13 over the conventional CG algorithm.
[19] Surface-fractal regime [8–11] above $q=a^{-1}$ is not clearly observed in the MD structure factor. Visualization revealed surface structures containing three-coordinated Si and single-coordinated O atoms.
[20] In the MD simulations, samples with different densities are prepared sequentially in the expansion schedule. The density dependence of the calculated quantities is therefore controlled by the history, and does not correspond exactly to those of experiments [8–11].
[21] T. A. Witten and L. M. Sander, Phys. Rev. Lett. **47**, 1400 (1981); P. Meakin, *ibid.* **51**, 1119 (1983); M. Kolb *et al.*, *ibid.* **51**, 1123 (1983); D. A. Weiz and M. Oliveria, *ibid.* **52**, 1433 (1984).

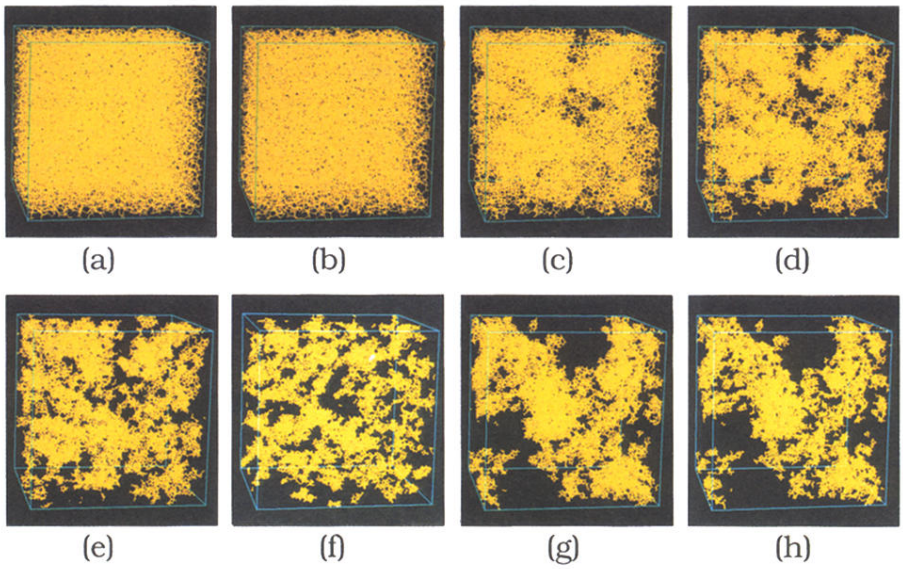

FIG. 1. Snapshots of MD porous SiO_2 glasses at densities (a) 2.2, (b) 1.6, (c) 0.8, (d) 0.4, (e) 0.2, and (f) 0.1 g/cm^3 prepared at 300 K, and (g) 0.2 and (h) 0.1 g/cm^3 prepared at 1000 K. Yellow lines represent Si-O bonds.